EXP5 - Analysis of Z^0-decays

Yannick Couzinié & Hannes Malcha

WS 2015/2016
02/15/2016 - 02/19/2016

Contents

1 Introduction **3**

2 Theoretical Background **3**
2.1 $\mathbf{e^-e^+}$ - Interactions and $\mathbf{Z^0}$ decay 3
2.1.1 Bhabha-Scattering 5
2.2 Forward-Backward-Asymmetry 6
2.3 Radiative Corrections 7

3 The OPAL-Detector **7**
3.1 Central Chambers 8
3.2 Calorimeters 8
3.2.1 Electromagnetic calorimeter 8
3.2.2 Hadron calorimeter 9
3.3 Muon detector 9

4 Data analysis **10**
4.1 Graphical analysis of $\mathbf{Z^0}$ decays 10
4.2 Statistical analysis of $\mathbf{Z^0}$ decays 10

5 Results and discussion **10**
5.1 Graphical analysis of $\mathbf{Z^0}$ decays 10
5.2 Analysis of Monte Carlo samples 12
5.3 Analysis of a real data sample 18
5.4 Lepton universality 25
5.5 Neutrino generations 26
5.6 Measurement of forward-backward asymmetry 27

6 Conclusion **29**

1 Introduction

In the course of this experiment we have analyzed Z^0 decays observed with the OPAL detector at the LEP e^-e^+-collider. For that we began with looking at single-event images for the various decay-modes of the Z^0-Boson. With these images and a set of simulated collisions we determined cuts to differentiate between the different decay modes. Using these cuts we then analyzed a large number of Z^0-decay events measured with the OPAL detector and determined the differential cross sections, mass of the Z^0 boson, the (partial) decay widths and the peak cross sections at resonance for the particular events. Finally we also find a value for the Weinberg-Angle and investigate the concept of lepton universality and the number of neutrino generations.

2 Theoretical Background

In this section we will briefly discuss the events we expect to observe and the formulas used for the calculations.

2.1 e^-e^+ - Interactions and Z^0 decay

In this experiment we wish to mainly observe the s-channel e^-e^+-interactions of the lowest order depicted in Fig. 1. The particles exchanged during the interaction are those of neutral currents, i.e. a Z^0 boson or a photon. To analyze the decay modes of the Z^0-boson the centre-of-mass energy $\sqrt{s}$ is (up to a few GeV) set to the rest energy of the particle. This leads to a Breit-Wigner-Resonance and thus making the creation of a Z^0-boson much more likely than a photon, upon annihilation of e^- with e^+. It can then decay into

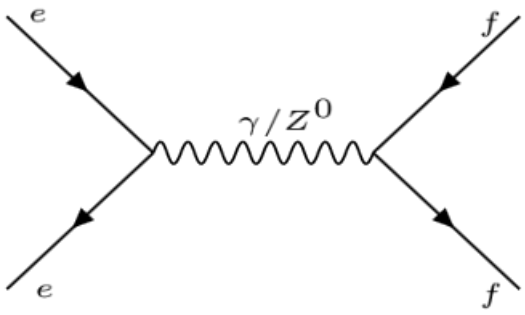

Figure 1: S-channel event for e^-e^+-interactions.

a pair of particles, in which the mass of the individual particles is smaller

than half of the mass of the Z^0-boson. That means we have the following possible final states of particles (that get created with their corresponding anti-particle):

- Charged leptons e, μ or τ.
- Neutrinos ν_e, ν_μ or ν_τ.
- Quarks u, d, s, c or b (the mass of the t-quark is too great to be created from the rest energy of the Z^0-boson alone).

One of the interesting attributes of a particle is (apart from its mass) its decay width. It is the direct sum of the partial widths

$$\Gamma_Z = \Gamma_e + \Gamma_{\nu_e} + \Gamma_\mu + \Gamma_{\nu_\mu} + \Gamma_\tau + \Gamma_{\nu_\tau} + \Gamma_u + \Gamma_d + \Gamma_c + \Gamma_s + \Gamma_b. \quad (2.1)$$

In the following formulas we are going to use the following terms

$$\text{Propagator } \chi(s) = \frac{s}{(s - M_Z^2) + is\Gamma_Z/M_Z}$$

$$\text{Colour-factor } N_C^f = \begin{cases} 1, & \text{for leptons} \\ 3, & \text{for quarks} \end{cases}$$

Charge in no. of elementary charges Q_f

Third component of weak isospin I_3^f

Sine squared of Weinberg-Angle $\sin^2\theta_W \approx 0.2312$[PDG14]

$$v_f = \frac{I_3^f - 2Q_f \sin^2\Theta_W}{2\sin\Theta_W \cos\Theta_W}$$

$$a_f = \frac{I_3^f}{2\sin\Theta_W \cos\Theta_W}$$

Fermi-constant $G_F = 1.1663 \cdot 10^{-5} GeV^{-2}$[PDG14]

Mass of Z^0 $M_Z = 91.187 GeV$[PDG14]

Since, in this experiment, we are only looking at centre-of-mass (CMS) energies around the rest mass of the Z^0-boson we obtain the following formula for the partial decay widths

$$\Gamma_f = \frac{\sqrt{2}N_c^f}{12\pi} G_F M_Z^3 ((I_3^f - 2Q_f \sin^2\Theta_W)^2 + I_3^{f2}). \quad (2.2)$$

Which gives us the results shown in Tab. 1 for the different decay modes. With eq. (2.2) we can now determine the cross sections

Channel	Partial width
$\Gamma_e = \Gamma_\mu = \Gamma_\tau$	83.4MeV
$\Gamma_{\nu_e} = \Gamma_{\nu_\mu} = \Gamma_{\nu_\tau}$	165.9MeV
$\Gamma_u = \Gamma_c$	285.4MeV
$\Gamma_d = \Gamma_s = \Gamma_b$	$367,9$MeV

Table 1: Theoretical results for the decay widths.

$$\sigma_f = \frac{12\pi\Gamma_e\Gamma_f}{M_Z^2 \cdot s}|\chi(s)|^2. \tag{2.3}$$

Which is the typical Breit-Wigner form of cross sections with the, already mentioned, resonance for $s \approx M_Z^2$. At the resonance eq. (2.3) yields

$$\sigma_f^{peak} \equiv \sigma_f|_{\sqrt{s}=M_Z} = \frac{12\pi}{M_Z^2}\frac{\Gamma_e\Gamma_f}{\Gamma_Z^2}, \tag{2.4}$$

thus we obtain the results listed in Tab. 2.

Channel	Peak cross section
$\sigma_e^{peak} = \sigma_\mu^{peak} = \sigma_\tau^{peak}$	2.09nb
$\sigma_{\nu_e}^{peak} = \sigma_{\nu_\mu} = \sigma_{\nu_\tau}$	4.14nb
$\sigma_u^{peak} = \sigma_c^{peak}$	7.16nb
$\sigma_d^{peak} = \sigma_b^{peak}$	9.23nb

Table 2: Theoretical results for the peak cross sections.

2.1.1 Bhabha-Scattering

The $e^-e^+ \to e^-e^+$ scattering process may either be the s-channel process depicted in Fig. 1 or the t-channel process depicted in Fig. 2 at lowest order. The differential cross sections for both these processes are different. For large values of Θ we expect mainly s-channel events with $\frac{\mathrm{d}\sigma}{\mathrm{d}\Omega} \propto (1+\cos^2\Theta)$, while for smaller values of Θ we expect mainly t-channel events with $\frac{\mathrm{d}\sigma}{\mathrm{d}\Omega} \propto (1-\cos\Theta)^{-2}$ (Θ being defined as the angle between ingoing and outgoing electron). We thus assume a total cross section of the form

$$\frac{\mathrm{d}\sigma}{\mathrm{d}\Omega} = a(1+\cos^2\Theta) + b(1-\cos\Theta)^{-2}\,. \tag{2.5}$$

Where a and b will be determined empirically later. It is crucial for our observations to know these values and to reduce the amount of t-channel

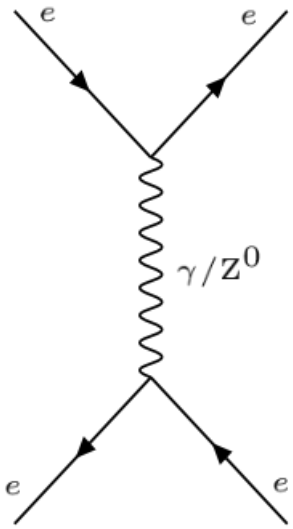

Figure 2: T-channel event for e^-e^+-interactions.

events to a relatively small amount, because in a t-channel event there is no Z^0-decay, we just observe an electron and a positron exchanging a neutral particle. Thus these events do not say anything about the decay modes of the Z^0-boson.

2.2 Forward-Backward-Asymmetry

For the $e^-e^+ \to f\overline{f}$ interactions ($f \neq e$) we have the differential cross sections given as

$$\frac{\mathrm{d}\sigma_f}{\mathrm{d}\Omega} = \frac{N_c^f}{4 \cdot 137^2 s} \left[F_1(s)(1+\cos^2\Theta) + 2F_2(s)\cos\Theta\right], \tag{2.6}$$

$$F_1(s) = Q_f^2 - 2v_e v_f Q_f \mathrm{Re}\chi + (v_e^2 + a_e^2)(v_f^2 + a_f^2)|\chi|^2, \tag{2.7}$$

$$F_2(s) = -2a_e a_f Q_f \mathrm{Re}\chi + 4v_e a_e v_f a_f |\chi|^2. \tag{2.8}$$

If we now calculate the proportions of particles scattered backwards and the ones scattered forward we obtain the following value known as the forward backward asymmetry

$$A_{FB}^f = \frac{\int_0^1 \frac{\mathrm{d}\sigma}{\mathrm{d}\cos\Theta}\mathrm{d}\cos\Theta - \int_{-1}^0 \frac{\mathrm{d}\sigma}{\mathrm{d}\cos\Theta}\mathrm{d}\cos\Theta}{\int_0^1 \frac{\mathrm{d}\sigma}{\mathrm{d}\cos\Theta}\mathrm{d}\cos\Theta + \int_{-1}^0 \frac{\mathrm{d}\sigma}{\mathrm{d}\cos\Theta}\mathrm{d}\cos\Theta} = \frac{3F_2}{4F_1}. \tag{2.9}$$

Where Θ is the angle between incoming and outgoing antiparticle. Some example values can be found in Tab. 3. Furthermore we find the following

	$\sin^2\Theta = 0.21$	$\sin^2\Theta = 0.23$	$\sin^2\Theta = 0.25$
$\sqrt{s} = 91.225GeV$	0.056	0.022	0.044
$\sqrt{s} = 89.225$	-0.094	-0.164	-0.195
$\sqrt{s} = 93.225$	0.231	0.196	0.190

Table 3: Theoretical values for A_{FB}^f calculated for lepton final states.

approximation for leptonic final states .

$$A_{FB}^{l,peak} \approx 3(v_l/a_l)^2 \tag{2.10}$$

Measuring the asymmetry at the resonance peak thus yields the Weinberg-Angle $\sin^2\Theta_W$.

2.3 Radiative Corrections

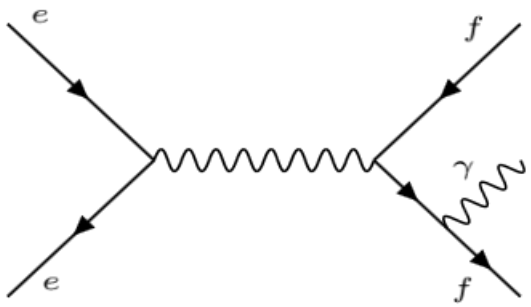

Figure 3: Second Order s-channel Feynman-diagram.

As per usual it does not suffice to only calculate the lowest orders of the processes. We have to account for the higher order Feynman-diagrams by correcting the cross sections. An example of a higher order process is given in Fig. 3. There are many more that will not be listed here. These higher order diagrams result in the radiative corrections for the cross sections listed in Tab. 4. These values are only approximations, but they will suffice for the accuracies we will have in our experiment, as the exact calculation would be a lot more cumbersome.

3 The OPAL-Detector

The Omni Purpose Apparatus for LEP (OPAL) experiment consisted of the detector shown in Fig. 4. We are going to briefly discuss the parts relevant

CMS energy $\sqrt{s}$ [GeV]	Hadronic corrections [nb]	Leptonic Corrections [nb]
88.47	+2.0	+0.09
89.46	+4.3	+0.20
90.22	+7.7	+0.36
91.22	+10.8	+0.52
91.97	+4.7	+0.22
92.96	-0.2	-0.01
93.71	-1.6	-0.08

Table 4: Radiative corrections for hadronic and leptonic final states.

for our experiment and how they measure the values we will examine. For more detailed information visit the official OPAL page [OPAL].

3.1 Central Chambers

The central jet chamber is a drift chamber (shown in red in Fig. 4). It is divided into 24 identical sectors each with 159 sense wires. The passing particles ionize the gas in the chamber, the resulting free electrons are then measured by the wires. This coupled with the curvature of charged particles in the magnetic field allows a measurement of the particle's momentum and a value for $\frac{\mathrm{d}E}{\mathrm{d}x}$.
Inside the central jet chamber lie the central vertex chamber (shown in magenta), and the innermost micro vertex detector. These are drift chambers used to locate short lived-particles and also to improve the momentum resolution. Finally there is the z chamber (in red around the jet chamber) which is a drift chamber with radial wires, which allows measurements of the z-component of the particle tracks.
The total momentum of the charged particles is $P_{charged}$ (in GeV) in the data to be analysed. The number of charged tracks measured in these chambers is $N_{charged}$.

3.2 Calorimeters

3.2.1 Electromagnetic calorimeter

The electromagnetic calorimeters (shown in cyan in Fig. 4) are mostly made of lead-glass blocks. Photons, electrons and positrons interact with the matter in these blocks, which causes electromagnetic showering. They have multiple radiations lengths so that most of the energy is deposited. The measured energy is given out as the value $ECAL$ (in GeV).

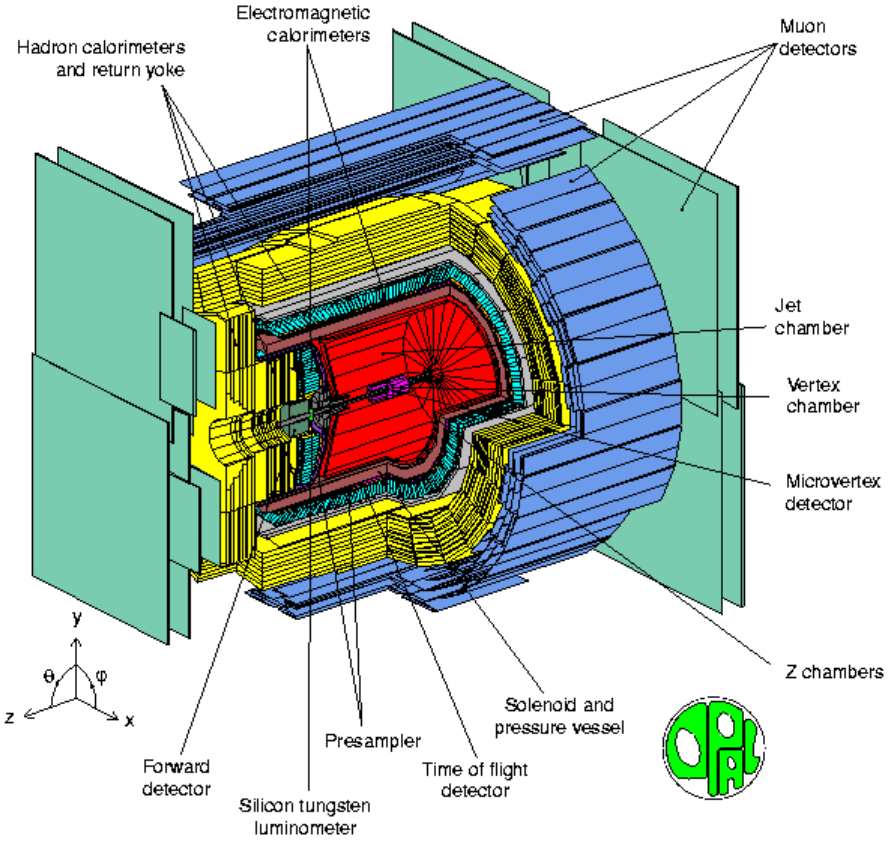

Figure 4: Cut-away view of the OPAL Detector [OPAL].

3.2.2 Hadron calorimeter

The hadronic calorimeter (shown in yellow) lies outside the electromagnetic calorimeter. It is composed of multiple layers of iron in which the hadrons emerging from the electromagnetic calorimeter, deposit most of their energy. The total energy deposited in the hadronic calorimeter is $HCAL$ (in GeV). Both calorimeters also help in the detection of muons as there is a (relatively) small energy deposited.

3.3 Muon detector

The muon detector (shown in blue in Fig. 4) consists of multiple layers of drift chambers. The muons are, apart from the neutrinos and other (unknown) rarely interacting particles, the only known particles that pass through both calorimeters. Since the muons deposit a relatively small amount of energy in both calorimeters a measurement in the muon detectors distinguishes muon

tracks from (e.g.) low energy hadron or neutrino tracks. The muons pass through the muon detector.

4 Data analysis

4.1 Graphical analysis of Z^0 decays

In the first part of the experiment we review different decay channels of the Z^0 boson event by event. These are separated into e^+e^-, $\mu^+\mu^-$, $\tau^+\tau^-$ and $q\overline{q}$ events. For each set we evaluate 20 events in terms of the variables $N_{charged}$, $P_{charged}$, $ECAL$ and $HCAL$ (see section 3). From this we draw histograms in order to prepare cuts to separate a set of mixed into pure events consisting of just one decay channel.

4.2 Statistical analysis of Z^0 decays

We are interested in measuring the cross section, mass and decay width of the Z^0 boson, as well as calculating the Weinberg-Angle, verifying Lepton universality and the number of light neutrino generations. Using a set of Monte Carlo simulated events we improve our previously developed cuts in order to investigate a real data sample later, which we will first separate into pure events using our cuts and then determine the values listed above.

5 Results and discussion

5.1 Graphical analysis of Z^0 decays

In Fig. 5 we present an example of the visualisation of a hadronic event measured in the OPAL detector.

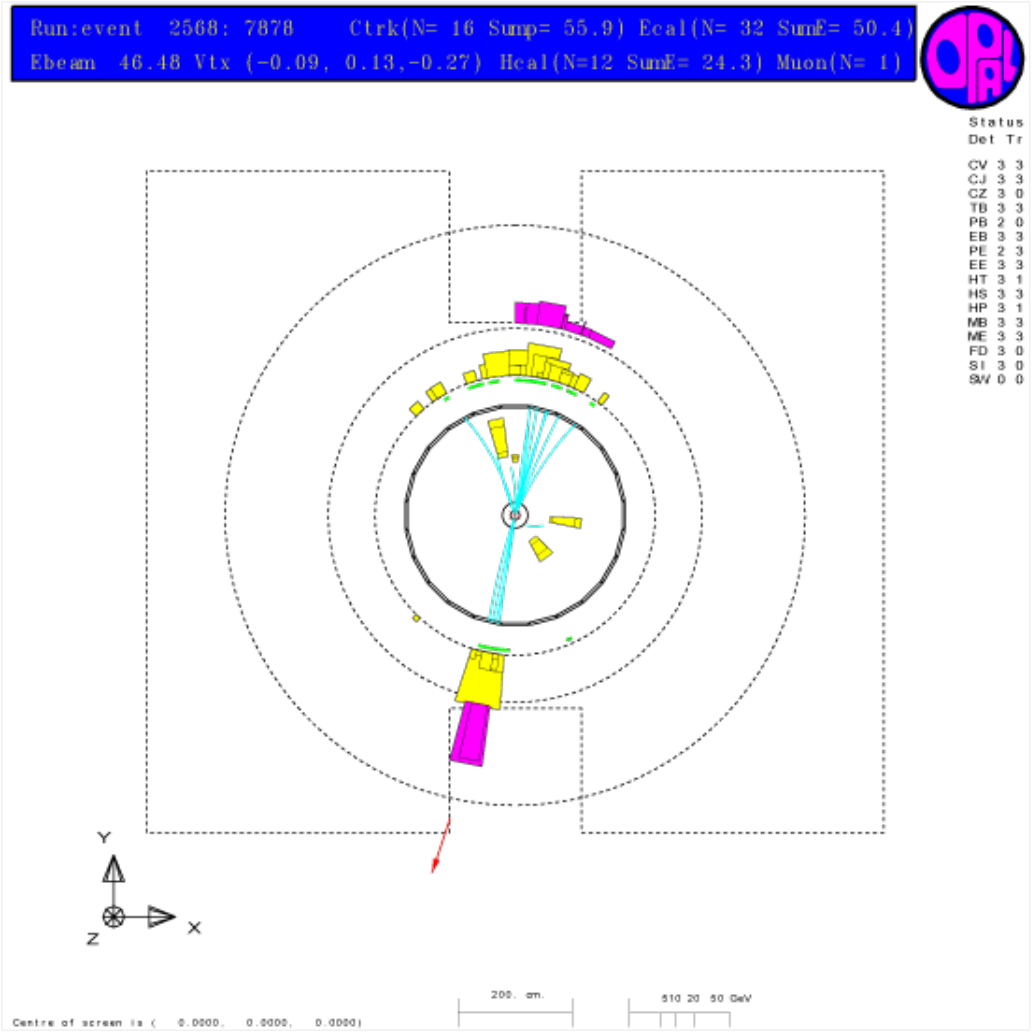

Figure 5: Hadron event in the OPAL detector with the measured deposited energy, momentum and number of charged particles.

The different decay modes of the Z^0 boson can be identified by looking at their visualisations in the OPAL detector. Lowest order electron events are always two particle decays and all the energy is deposited in the electronic calorimeter. Muons on the other hand only deposit a fraction of their energy in both calorimeters and then escape from the detector. But as the electron events they are always two particle decays. Tauons almost instantaneously decay into two or more particles, which means that, in contrast to the electronic and muonic channel, one sees the tauon particle-antiparticle pair which then decays into pions, muons or electrons signified by a change in the momentum of the charged particle (as the resulting neutrinos cannot

Decay mode	Partial decay width
$\pi^-\pi^0\nu_\tau$	$(25.52 \pm 0.09)\%$
$e^-\overline{\nu}_e\nu_\tau$	$(17.83 \pm 0.04)\%$
$\mu^-\overline{\nu}_\mu\nu_\tau$	$(17.41 \pm 0.04)\%$
$\pi^-\nu_\tau$	$(10.83 \pm 0.06)\%$
$\pi^-\pi^+\pi^-\nu_\tau$	$(9.31 \pm 0.06)\%$
$\pi^-\pi^+\pi^-\pi^0\nu_\tau$	$(4.62 \pm 0.06)\%$
$\pi^-3\pi^0\nu_\tau$	$(1.05 \pm 0.07)\%$

Table 5: Decay modes with the highest partial decay widths for the tauon as listed in [PDG14].

be observed). A list of the most probable decays for tauons as listed by the particle data group can be seen in Tab. 5. Quarks immediately hadronize which results in so called jets, which give the signal of usually more than 10 charged tracks of hadrons and leptons going in the same general direction. They deposit most of their energy in the ECAL and HCAL. Besides all of these regular events one must bear in mind the existence of other events like the decay of atmospheric muons in the detector. These events can be recognized easily since they do not originate from the center where the electrons and positrons collide. The preliminary cuts we determined from the purely visual analysis can be seen in Tab. 6. For the rest of the experiment we will no further survey visualizations but data sets of multiple thousand collisions at the same time.

	e^+e^-	$\mu^+\mu^-$	$\tau^+\tau^-$	$q\overline{q}$
$ECAL$	$[80, 1000]$	$[0, 5]$	$[0, 1000]$	$[0, 1000]$
$HCAL$	$[0, 1]$	$[1, 1000]$	$[1, 1000]$	$[1, 1000]$
$N_{charged}$	$[0, 5]$	$[0, 5]$	$[0, 5]$	$[5, 1000]$
$P_{charged}$	$[0, 60]$	$[82, 1000]$	$[0, 60]$	$[0, 1000]$

Table 6: Cuts from the visual analysis of a selection of 20 events for each decay channel. 1,000 is an arbitrary large number to include all events.

5.2 Analysis of Monte Carlo samples

To start we will use electron positron collision events, which were simulated using the Monte Carlo Method, to mimic the real events in the OPAL detector. They are used for improving the real data analysis since they are already separated in sets of pure events. They provide information about the proportion of background and missed events. It is very important that

the simulation is as precise as possible in order to avoid uncertainties in later measurements and cuts. We investigate Monte Carlo samples with 100,000 simulated events. These events pass preselection cuts before they are available to us, so we see less than 100,000 events.
At first we look at a sample only containing electron events. These can either be s- or t-channel events. The differential cross section of the two channels depends on the angle between the incoming and outgoing electron. In our final data we want only 5% of the electron events to be t-channel events, as we reckon this is a good trade-off between maximizing the amount of s-channel events and minimizing the amount of t-channel events. Therefore we fit eq. (2.5) to the Monte Carlo data in order to obtain the two constants a and b. This is done using the program ROOT [ROOT], in which we enter the function (2.5) and the program then chooses the values a and b in order to fit the function to the values displayed in Fig. 6. We obtain $a = 19.85 \pm 0.2$ and $b = 2.85 \pm 0.1$. Due to some construction issues with the detector we also cut out events with angles between $\cos(\theta) = -1$ and $\cos(\theta) = -0.925$, $\cos(\theta) = -0.85$ and $\cos(\theta) = -0.7$ and $\cos(\theta) = 0.7$ and $\cos(\theta) = 1$ (see Fig. 6). Instead of generally following the curve given by eq. (2.5), we observed unexpected behavior and thus decided to leave out these angle ranges, as it is known, that there are angle ranges in the OPAL detector which are not usable for scientific experimentation in these electronic decay channels.

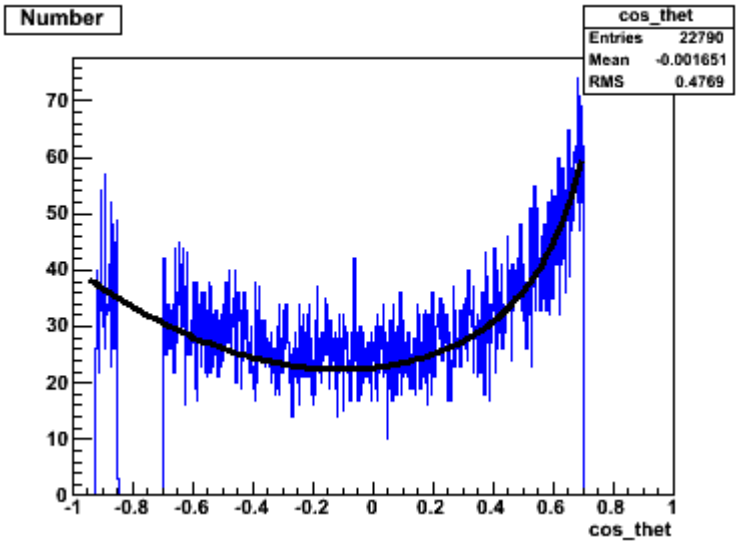

Figure 6: Number of electron events in Monte Carlo sample dependent on the angle between incoming and outgoing electron.

Now we determine the value for $\cos(\theta)$ so that the data only contains 5% t-channel events. Thus we say the number of t-channel events divided by the total number of events shall be 0.05. The variable in this equation is the upper integration boundary y, the θ_i are the angle ranges that we took out because of the detector properties (see above). We obtain

$$\begin{aligned}
& \frac{\text{Number of t-channel events in angle range } [\cos\theta_1, y]}{\text{Total number of electron events in angle range } [\cos\theta_1, y]} \stackrel{!}{=} 0.05 \\
\Leftrightarrow \quad & \frac{\int_{\cos\Theta_1}^{\cos\Theta_2} b(1-\cos\Theta)^{-2}\,\mathrm{d}\cos\Theta + \int_{\cos\Theta_3}^{y} b(1-\cos\Theta)^{-2}\,\mathrm{d}\cos\Theta}{\int_{\cos\Theta_1}^{\cos\Theta_2} \frac{d\sigma}{d\Omega}\,\mathrm{d}\cos\Theta + \int_{\cos\Theta_3}^{y} \frac{d\sigma}{d\Omega}\,\mathrm{d}\cos\Theta} = 0.05 \\
\Leftrightarrow \quad & \frac{\int_{-0{,}925}^{-0.85} \frac{2.85}{(1-x)^2}\,\mathrm{dx} + \int_{-0.7}^{y} \frac{2.85}{(1-x)^2}}{\int_{-0.925}^{-0.85} 19.85(1+x^2) + \frac{2.85}{(1-x)^2}\,\mathrm{dx} + \int_{-0.7}^{y} 19.85(1+x^2) + \frac{2.85}{(1-x)^2}\,\mathrm{dx}} = 0.05 \\
\Leftrightarrow \quad & \frac{0.006 - \frac{2.85}{y-1} - \frac{2.85}{1.7}}{2.723 + 6.618y^3 + 19.854y - \frac{2.85}{y-1} + 14.491} = 0.05 \\
\Leftrightarrow \quad & y = -0.12562\,.
\end{aligned} \tag{5.1}$$

From now on we will use this value whenever investigating electron events to make sure we only have 5% t-channel events.

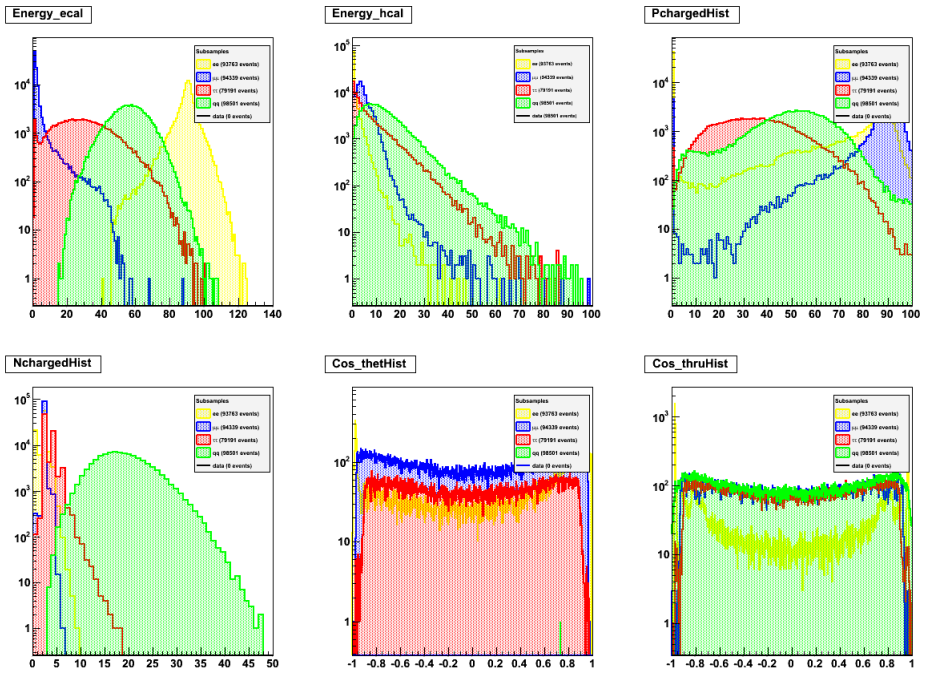

Figure 7: Uncut sample of Monte Carlo Events. Yellow: e^-e^+, Blue: $\mu^-\mu^+$, Red: $\tau^-\tau^+$, Green: $q\overline{q}$.

In Fig. 7 one can see the data from a Monte Carlo sample of 100,000 events. As already elucidated we are mostly interested in the ECAL (top left), HCAL (top centre), the momentum of the charged particles ($P_{charged}$) (top right), the number of charged particles ($N_{charged}$) (bottom left) and for the electron events the angle between incoming and outgoing positrons ($\cos(\theta)$) (bottom center). In a real data sample the different types of events will not be coloured, so we will need to cut the histograms to obtain pure events. This of course does not work perfectly. There is always a loss in relevant events and a background of different events. The accomplished accuracy is mathematically expressed in the so called efficiency matrix. By examining the data from Fig. 7 we define the cuts listed in Tab. 7.

	e^+e^-	$\mu^+\mu^-$	$\tau^+\tau^-$	$q\overline{q}$
$ECAL$	$[80, 1000]$	$[0, 24]$	$[0, 65]$	$[14, 110]$
$HCAL$	$[0, 0.5]$	$[0, 20]$	$[0, 1000]$	$[0, 1000]$
$N_{charged}$	$[0, 2]$	$[0, 2]$	$[0, 6]$	$[10, 1000]$
$P_{charged}$	$[0, 1000]$	$[70, 1000]$	$[5, 70]$	$[0, 1000]$

Table 7: Cuts from the Monte Carlo sample for separating any sample. 1,000 is an arbitrary big number to include all events.

We now apply the cuts on the simulated data and obtain the number of events which passed the cuts for each decay channel. This number is divided by the total number of events before applying the cuts. In the electronic decay channel, we used the number obtained after applying the angle ranges (i.e. $19,020$ events) which were found in eq. (5.1), because we are only going to measure the s-channel events (as already discussed above). The findings are written down as a matrix. Thus the ε_{11} entry is the percentage of electrons which pass the electron cuts. ε_{21} is the percentage of muons which pass the electron cuts. ε_{31} is the percentage of taouns which pass the electron cuts. And ε_{41} is the percentage of hadrons which pass the electron cuts. The second column is for the muon cuts, the third for the tauon cuts and the last for the hadronic cuts. The numbers from our measurement to determine the efficiency matrix are listed in Tab. 8

	$e-$cuts	μ-cuts	τ-cuts	q-cuts
e^+e^-	7,969	0	149	0
$\mu^+\mu^-$	0	56,840	2,820	0
$\tau^+\tau^-$	4	79	73,627	148
$q\overline{q}$	0	0	224	95,246

Table 8: Number of events from the Monte Carlo sample which pass the cuts from Tab. 7. The total number of events is 19,020 for electrons, 94,399 for muons, 79,191 for tauons and 98,501 for hadrons.

With the results from Tab. 8 we compute the efficiency matrix as explained above, and yield

$$\varepsilon = \begin{pmatrix} 0.419 & 0 & 0.00005 & 0 \\ 0 & 0.603 & 0.001 & 0 \\ 0.008 & 0.030 & 0.930 & 0.002 \\ 0 & 0 & 0.002 & 0.967 \end{pmatrix} . \tag{5.2}$$

The matrix serves the following equation

$$\begin{aligned} \vec{N}_{obs} &= \varepsilon \cdot \vec{N}_{true} \\ \Leftrightarrow \begin{pmatrix} N_{e,obs} \\ N_{\mu,obs} \\ N_{\tau,obs} \\ N_{h,obs} \end{pmatrix} &= \varepsilon \cdot \begin{pmatrix} N_{e,true} \\ N_{\mu,true} \\ N_{\tau,true} \\ N_{h,true} \end{pmatrix} . \end{aligned} \tag{5.3}$$

With $N_{f,obs}$ being the number of observed events after applying a cut to a sample and $N_{f,true}$ being the real number of events that occurred. For an ideal cut, with no background, we would have a passing rate of 100% and ε would be the identity matrix. The uncertainty of the efficiency matrix is calculated with the equation

$$\sigma_{ij,\,\varepsilon} = \sqrt{\frac{\varepsilon_{ij}(1-\varepsilon_{ij})}{N}} \,. \tag{5.4}$$

Later we will be interested in the inverse of the efficiency matrix and its uncertainty since we measure $N_{f,obs}$ and are interested in calculating $N_{f,true}$. We find

$$\begin{aligned} & \varepsilon\varepsilon^{-1} && = 1 \\ \Leftrightarrow \quad & \Delta\left(\varepsilon\varepsilon^{-1}\right) && = \Delta 1 \\ \Leftrightarrow \quad & (\Delta\varepsilon)\,\varepsilon^{-1} + \varepsilon\left(\Delta\varepsilon^{-1}\right) && = 0 \\ \Leftrightarrow \quad & \varepsilon^{-1}\,(\Delta\varepsilon)\,\varepsilon^{-1} + \varepsilon^{-1}\varepsilon\left(\Delta\varepsilon^{-1}\right) && = 0 \\ \Leftrightarrow \quad & \Delta\varepsilon^{-1} && = -\varepsilon^{-1}\,(\Delta\varepsilon)\,\varepsilon^{-1} \,. \end{aligned} \tag{5.5}$$

So

$$\sigma_{\varepsilon^{-1}} = \varepsilon^{-1}\sigma_{\varepsilon}\,\varepsilon^{-1} \,. \tag{5.6}$$

This yields

$$\varepsilon^{-1} = \begin{pmatrix} 2.387 & 6.43 \cdot 10^{-6} & -0.0001 & 30.497 \cdot 10^{-6} \\ 33.23 \cdot 10^{-6} & 1.660 & -0.002 & 4.19 \cdot 10^{-6} \\ -0.020 & -0.053 & 1.076 & -0.003 \\ 38.87 \cdot 10^{-6} & 0.0001 & -0.002 & 1.034 \end{pmatrix} \tag{5.7}$$

and

$$\sigma_{\varepsilon^{-1}} = 10^{-6} \begin{pmatrix} 20,379 & 3.26 & 63.60 & 169.76 \\ 6.06 & 4,378 & 0.0002 & 73.29 \\ 1,450 & 7,970 & 10,421 & 1,649 \\ 5.97 & 9.95 & 167 & 608 \end{pmatrix} \tag{5.8}$$

All diagonal elements have a small uncertainty and most of the off-diagonal elements do as well. Only the distinction between muon and tau events carries a high uncertainty.

5.3 Analysis of a real data sample

At this point we have prepared all the necessary tools for analyzing a real data sample. We were provided with multiple data sets (labeled by number), of which we will analyze the first (data 1). In this particular sample the Z^0 decay was measured at 7 different centre-of-mass energies with the individual integrated luminosities and their respective uncertainties listed in Tab. 10. To obtain only events with those energies we had to make cuts to the allowed centre-of-mass energy which are displayed in Tab. 9.

Energy [GeV]	$E_{lower}[GeV]$	$E_{upper}[GeV]$
88.48021	88.48	88.49
89.47158	89.47	88.48
90.22720	90.22	90.23
91.23223	91.23	91.24
91.97109	91.97	91.98
92.97091	92.97	92.98
93.71841	93.71	93.72

Table 9: Cuts used to differentiate between the events for different centre-of-mass-energies.

Energy [GeV]	Int. Luminosity $[(\text{nb})^{-1}]$	Uncertainty $[(\text{nb})^{-1}]$
88.48021	675.8590	5.721257
89.47158	543.6270	4.830643
90.22720	419.7760	3.974844
91.23223	3122.204	22.31760
91.97109	639.8380	5.577354
92.97091	479.2400	4.481870
93.71841	766.8380	6.497519

Table 10: Properties of the real data sample used for further measurements and calculations.

We now apply our cuts to the real data sample at each of the seven centre-of-mass energies. This gives us a vector with four entries, one for each set of cuts we made. This vector represents the observed values from eq. (5.3) $\vec{N}_{obs,CMS}$ Where CMS is one of the seven Center-of-mass energies from Tab.

10 in the order they are presented in the table. So the observed values are

$$\vec{N}_{obs,1} = \begin{pmatrix} 28 \\ 133 \\ 164 \\ 3,443 \end{pmatrix}, \quad \vec{N}_{obs,2} = \begin{pmatrix} 14 \\ 74 \\ 220 \\ 1,253 \end{pmatrix}, \quad \vec{N}_{obs,3} = \begin{pmatrix} 32 \\ 132 \\ 277 \\ 2818 \end{pmatrix},$$

$$\vec{N}_{obs,4} = \begin{pmatrix} 824 \\ 3,834 \\ 3,790 \\ 89,925 \end{pmatrix}, \quad \vec{N}_{obs,5} = \begin{pmatrix} 113 \\ 676 \\ 631 \\ 14,937 \end{pmatrix}, \quad \vec{N}_{obs,6} = \begin{pmatrix} 36 \\ 160 \\ 276 \\ 3,769 \end{pmatrix},$$

$$\vec{N}_{obs,7} = \begin{pmatrix} 50 \\ 195 \\ 307 \\ 4,261 \end{pmatrix}.$$

By multiplying the inverse efficiency matrix with one of these vectors we obtain the values for each decay channel after the preselection by the detector, as this is how the entries of the efficiency matrix were calculated (from preselection trigger event numbers to event numbers after cuts, the inverse just does the inverse). This follows directly from eq. (5.3). Additionally we know the ratio of events that do not pass the preselection triggers of the detector from the simulated events. We calculate this corrective factor by dividing the total amount of simulated events by the total amount of measured simulated events, and apply that to the calculated values $\varepsilon^{-1}\vec{N}_{obs}$. For example, as can be seen in Fig. 7, only 93,763 electron events pass the preselection cuts. That means we obtain a corrective factor for the electrons of

$$\frac{100000}{93763} = 1.066518776.$$

All the corrective factors are listed in Tab. 11.

Decay channel	Measured events	Resulting corrective factor
e^-e^+	93763	1.066518776
$\mu^-\mu^+$	94339	1.060006996
$\tau^-\tau^+$	79191	1.2627697592
$q\overline{q}$	98501	1.0152181196

Table 11: Corrective values due to the preselection made by the detector (trigger levels), calculated using the values for the simulated events seen in Fig. 7.

These particular values are now multiplied to each of the values of $(\varepsilon^{-1}\vec{N}_{obs})_i$ to obtain the true value for the number of events of a particular decay channel

$\vec{N}_{true,i}$.
We still need to calculate the total uncertainty for those true values. For the measurement of $\vec{N}_{obs}$ we assume a Poisson distribution and thus estimate the uncertainty at $\sqrt{N}$. This is combined with the uncertainty that results from the multiplication with the inverse efficiency matrix from eq. (5.8). With error propagation it follows that

$$\sigma_{(\varepsilon^{-1}\vec{N}_{obs})_i} = \sqrt{\sum_{j=1}^{4} \left((\sigma_{\varepsilon^{-1}})_{ij} (\varepsilon^{-1}\vec{N}_{obs})_j \right)^2 + \left(\varepsilon_{ij}^{-1} \sigma_{N_{obs,j}} \right)^2}. \tag{5.9}$$

And finally we have to multiply these error margins with the corrective factors from the preselection cuts to obtain the uncertainties for the number of particular decay channel events in $\vec{N}_{true}$. This calculation is repeated for each of the seven CMS energies. The results are presented in Tab. 12, out of which we would like to emphasize the relatively high number of quark decay events (at least 5 times bigger than the next bigger value (tauon decays)).

	e^-e^+	$\mu^-\mu^+$	$\tau^-\tau^+$	$q\overline{q}$
88.48 GeV	71 ± 14	234 ± 20	202 ± 17	$3,615 \pm 62$
89.47 GeV	36 ± 10	130 ± 15	289 ± 20	$1,315 \pm 37$
90.23 GeV	82 ± 15	232 ± 20	358 ± 23	$2,958 \pm 56$
91.23 GeV	$2,099 \pm 85$	$6,739 \pm 113$	$4,581 \pm 86$	$94,406 \pm 320$
91.9711 GeV	288 ± 28	$1,188 \pm 46$	761 ± 34	$15,702 \pm 129$
92.9709 GeV	92 ± 15	281 ± 22	351 ± 23	$3,957 \pm 65$
93.72 GeV	127 ± 18	343 ± 25	389 ± 24	$4,473 \pm 69$

Table 12: Calculated true values for each decay mode and CMS energy at real data sample.

Using these values we compute the cross section for the hadronic and leptonic channels and with error propagation we obtain

$$\sigma = \frac{N_{true}}{L_{int}} \tag{5.10}$$

$$\sigma_\sigma = \sigma \cdot \sqrt{\left(\frac{\sigma_N}{N}\right)^2 + \left(\frac{\sigma_{L_{int}}}{L}\right)^2} \tag{5.11}$$

Bearing in mind the radiative correction from Tab. 4, which we added to the cross sections of the particular decay channels, this leads us to Tab. 13.

$\sqrt{s}$	e^-e^+	$\mu^-\mu^+$	$\tau^-\tau^+$	$q\bar{q}$
88.48 GeV	0.20 ± 0.04	0.44 ± 0.04	0.39 ± 0.03	7.4 ± 0.1
89.47 GeV	0.27 ± 0.07	0.44 ± 0.05	0.73 ± 0.05	6.72 ± 0.2
90.23 GeV	0.6 ± 0.1	0.91 ± 0.08	1.21 ± 0.08	14.75 ± 0.3
91.23 GeV	1.19 ± 0.05	2.68 ± 0.05	1.99 ± 0.04	41.0 ± 0.3
91.9711 GeV	0.67 ± 0.06	2.08 ± 0.08	1.41 ± 0.06	29.2 ± 0.3
92.9709 GeV	0.18 ± 0.03	0.58 ± 0.05	0.72 ± 0.05	8.1 ± 0.2
93.72 GeV	0.09 ± 0.01	0.37 ± 0.03	0.43 ± 0.03	4.2 ± 0.1

Table 13: Measurement of cross sections at different centre of mass energies for all decay modes. Values provided in *nb*.

A Breit-Wigner curve is now fitted to the results using the program ROOT [ROOT] and a C++-script. The results can be seen in Fig. 8 to 11.

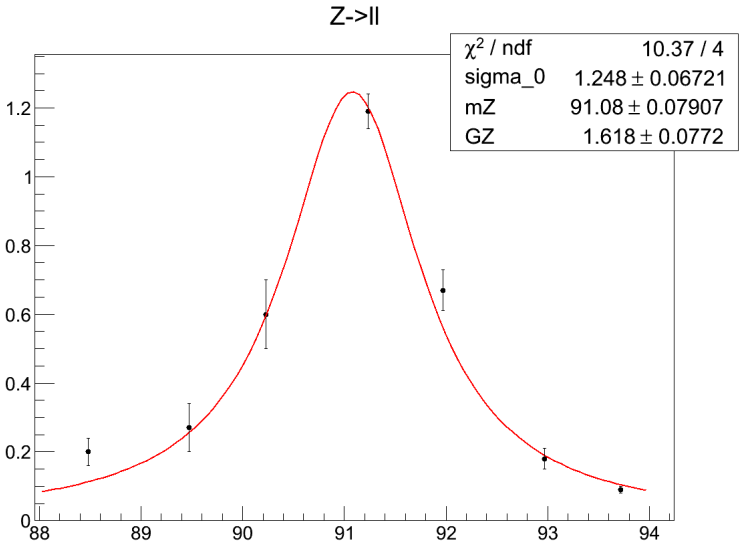

Figure 8: Fit of the electron values from Tab. 13 to a Breit Wigner distribution.

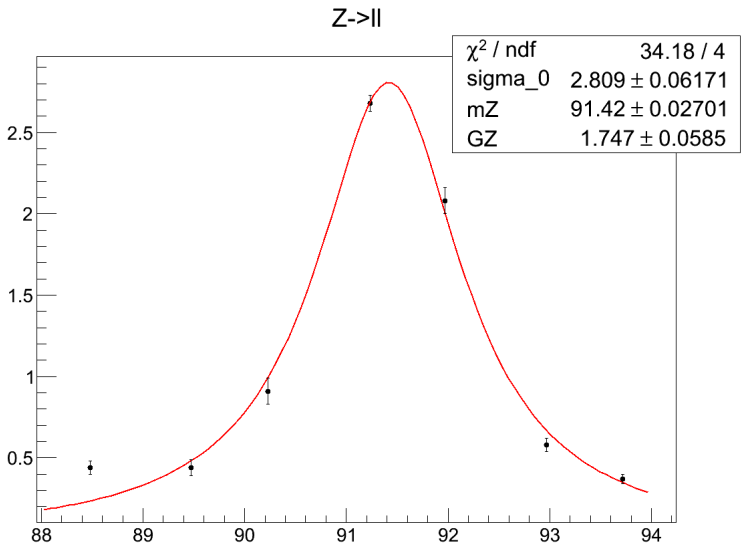

Figure 9: Fit of the muon values from Tab. 13 to a Breit Wigner distribution.

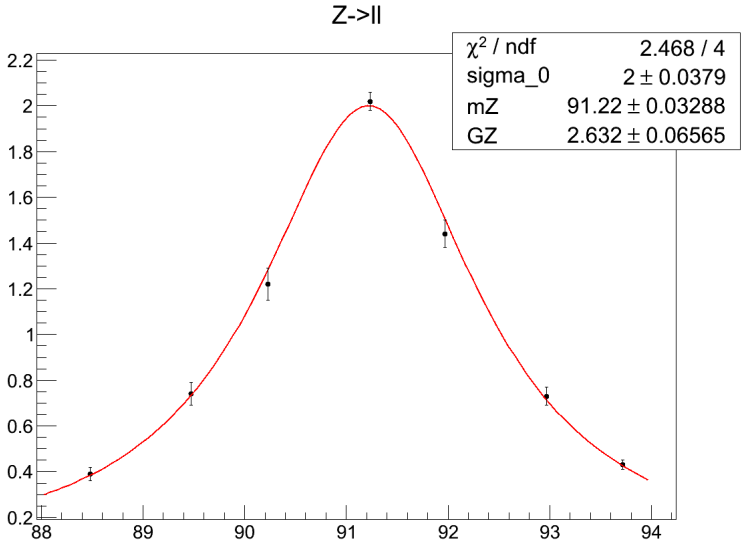

Figure 10: Fit of the tauon values from Tab. 13 to a Breit Wigner distribution.

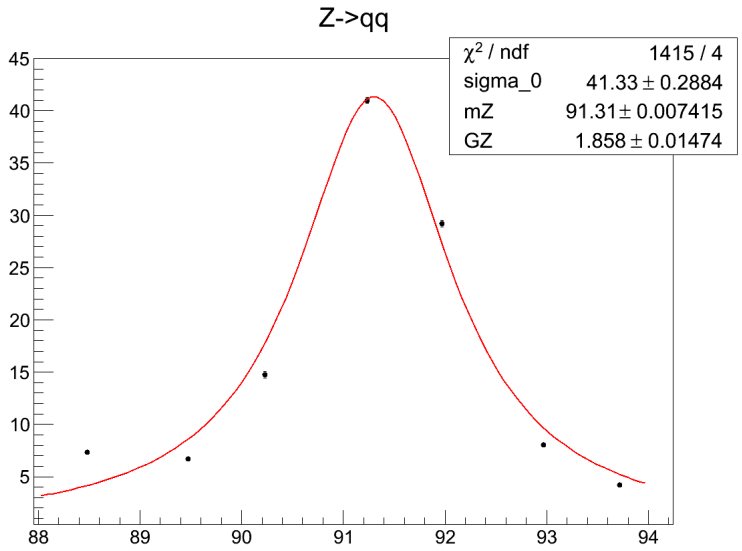

Figure 11: Fit of the hadron values from Tab. 13 to a Breit Wigner distribution.

The fitting script provides us with the values χ^2, σ_f^{peak}, the mass of the Z^0 boson m_Z and the total decay width of the Z^0 boson Γ_Z. Obviously all fits have four degrees of freedom since there are three unknown values in eq. 2.3 and we have seven measurement points. The reduced χ^2 value is a benchmark for the quality of the fit. Commonly a so called cutoff p-value is used to distinguish between significant and insignificant results. Usually the cutoff p-value is chosen to be 5%. In Tab. 14 we have listed the $1-p$ values for each fit.

Event	χ^2/ndf	Probability $(1-p)$
e^-e^+	2.59	62.86%
$\mu^-\mu^+$	8.55	7.34%
$\tau^-\tau^+$	0.62	96.08%
$q\overline{q}$	353.75	$2.7 \cdot 10^{-75}$

Table 14: Probability for measured values from Fig. 8 to 11 to be correct.

In these terms the data from the tauon events is the only significant one, i.e. with $p \leq 5\%$. The hadronic channel has very small error margins, which leads to the small value for p shown in Tab. 14. We believe this to be due to the relatively high amount of hadron channel events (see Tab. 12), because we assumed a Poisson distribution, which results in lower relative errors for channels with more events $\left(\frac{\sigma}{N} = \frac{1}{\sqrt{N}}\right)$. Small error margins with non-ideal

agreement between theoretical and empirical values lead to large χ^2, which we observe here.
In Tab. 15 we compare the measured values for the peak cross sections, to the values listed in the PDG and theoretical values we calculated earlier (presented in Tab. 2, where one has to add the different hadronic channel cross sections together). The results can be seen in Tab. 15.

	Reading	PDG	Theoretical Value
e^-e^+	1.248 ± 0.007	1.996 ± 0.007	2.093
$\mu^-\mu^+$	2.81 ± 0.06	1.998 ± 0.006	2.093
$\tau^-\tau^+$	2.00 ± 0.04	2.000 ± 0.007	2.093
$q\overline{q}$	41.3 ± 0.3	41.54 ± 0.04	42.018

Table 15: Comparison of measured data for the peak cross sections σ_f in nb from the Breit-Wigner fit to values from PDG and theoretical values from Tab. 2.

Using eq. (2.4) we now calculate the partial widths of the decay channels. We thus solve it for Γ_f, and obtain

$$\Gamma_e = \sqrt{\frac{\sigma_f^{peak}\Gamma_Z^2 M_Z^2}{12\pi}} \tag{5.12}$$

$$\Gamma_f = \frac{\sigma_f^{peak} M_Z^2 \Gamma_Z^2}{12\pi\Gamma_e} \tag{5.13}$$

With error propagation we obtain for the error margins

$$\sigma_{\Gamma_e} = \Gamma_e \sqrt{\left(\frac{\sigma_{\sigma_e^{peak}}}{2\sigma_e^{peak}}\right)^2 + \left(\frac{\sigma_{M_Z}}{M_Z}\right)^2 + \left(\frac{\sigma_{\Gamma_Z}}{\Gamma_Z}\right)^2}, \tag{5.14}$$

$$\sigma_{\Gamma_f} = \Gamma_f \sqrt{\left(\frac{\sigma_{\Gamma_e}}{\Gamma_e}\right)^2 + \left(\frac{\sigma_{\sigma_f^{peak}}}{\sigma_f^{peak}}\right)^2 + \left(\frac{2\sigma_{M_Z}}{M_Z}\right)^2 + \left(\frac{2\sigma_{\Gamma_Z}}{\Gamma_Z}\right)^2}. \tag{5.15}$$

We calculate the partial width of the electron decay channel first to obtain values for the remaining decay modes. For the values of Γ_Z and m_Z we use the mean value of all the fits, i.e.

$$m_Z = 91.26\text{GeV} \pm 0.02\text{GeV},$$
$$\Gamma_Z = 1.96\text{GeV} \pm 0.03\text{GeV}.$$

Where the errors are calculated with error propagation. As this calculation for the uncertainties is the same for all averaged values, we will explain it

generally here, and it is to be assumed implicitly from now on that we used this formula to calculate the uncertainty of an averaged value. Let a_i be a set of N measured values for the same value a. Let σ_i be the uncertainty of the particular values of a_i. We thus yield for the average and the uncertainty for a using error propagation

$$a = \frac{1}{N} \sum_{i=1}^{N} a_i \tag{5.16}$$

$$\sigma_a = \frac{1}{N} \sqrt{\sum_{i=1}^{N} \sigma_i^2} \tag{5.17}$$

We obtain the results for the partial widths listed in Tab. 16.

	Reading	PDG	Theoretical Value
$e^- e^+$	0.052 ± 0.0008	0.0839 ± 0.0001	0.083
$\mu^- \mu^+$	0.118 ± 0.005	0.0840 ± 0.0002	0.083
$\tau^- \tau^+$	0.084 ± 0.003	0.0841 ± 0.0002	0.083
$q\overline{q}$	1.73 ± 0.06	1.744 ± 0.002	1.6753

Table 16: Comparison of measured data for the partial widths Γ_f in GeV, calculated with eq. (5.12) and (5.13) from the Breit-Wigner fit to values from PDG and theoretical values from Tab. (1).

The result for the mass of the Z^0 boson is in the 4σ range of the respective measured PDG value of $91.188 \pm 0.002\ GeV$. The reading for the total decay width (PDG: $2.495 \pm 0.002\ GeV$) on the other hand, as well as the partial decay width and the cross section for the electron and muon events differ up to $\sim 40\sigma$ from the expected results. As expected the readings for the tau events are all relatively good (in the 1σ range of the expected values). Surprisingly the hadronic reading fit the expected values just as well. We assume this to be due to the high number of hadronic events in the detector. It is very important to emphasize that the partial decay widths were calculated using the readings for the total decay width, mass and cross sections of the Z^0 boson. As illustrated some of these values are far away from the theoretical predictions so agreements with theoretical values for the partial decay width are likely to be accidental.

5.4 Lepton universality

We will now verify lepton universality using the calculated cross sections in Tab. 15. This concept implies that the total cross section at resonance

should be the same for all leptons. As discussed before only the value for the tauons fits the expected value. Respective lepton universality can not be verified using our data since the readings vary up to 55% of the theoretical value. The theoretical value of $\sigma_l^{peak} = 2.093\,nb$ is in the 4σ range of the mean value of all leptonic cross sections at resonance

$$\sigma_l^{peak} = \frac{\sigma_l^{peak} + \sigma_\mu^{peak} + \sigma_\tau^{peak}}{3} = (2.02 \pm 0.02)\,nb\,. \tag{5.18}$$

If we calculate the mean value of the total cross section for all leptons and consider the quotient between the lepton and the hadron branching ratio we obtain the following results

$$\frac{\sigma_l^{peak}}{\sigma_h^{peak}} = 0.0489 \pm 0.0007\,. \tag{5.19}$$

This is in the 2σ range of the expected value of 0.0498. The relatively low error margin is again explained in the high amount of hadron events. Finally the diversions from the respective expected values do suggest that our cuts might not have been exact enough.

5.5 Neutrino generations

A recurring question in modern particle physics is the question for the number of neutrino generations. It is assumed in the standard model, that all leptons come in doublets, which is a rule based on empirical evidence, rather than theoretical principles. If we assume that there are only 3 charged lepton families and 3 quark families we can obtain a value for the number of neutrino generations N_ν with

$$N_\nu = \frac{\Gamma_Z - \Gamma_e - \Gamma_\mu - \Gamma_\tau - \Gamma_q}{\Gamma_\nu}\,, \tag{5.20}$$

$$\sigma_{N_\nu} = \frac{\sqrt{\sigma_{\Gamma_e}^2 + \sigma_{\Gamma_\mu}^2 + \sigma_{\Gamma_\tau}^2 + \sigma_{\Gamma_q}^2 + \sigma_{\Gamma_Z}^2}}{\Gamma_\nu}\,. \tag{5.21}$$

We can examine this with the measured values from Tab. 16 which lists all the necessary measured values to evaluate this number. As only the tauon measurements have shown χ^2/ndf values which are statistically relevant we will restrict ourselves to the results from that measurement. Thus we obtain

$$N_\nu = 3.9 \pm 0.5\,. \tag{5.22}$$

The theoretical value of 3 lies in the 2σ range of our calculated value however the uncertainty on our value is about 13%. Considering the strong empirical evidence for 3 neutrino generations measured up until now coupled with the relatively high error margins on our measured values we do not think we can confirm the expected value nor propose a new value.

5.6 Measurement of forward-backward asymmetry

As described in section 2.2 we can use the equation (2.10) to measure the value $\sin^2\Theta_W$ by measuring the forward backward asymmetry at the resonance peak ($s \approx M_Z^2$). This means that in this section we limit ourselves to the analysis of the data sets with CMS energies closest to M_Z^2, i.e. for the three data sets (1-3) in GeV we use the CMS-energies 91.23223, 91.23965, 91.22910. Since the muonic decay channel of the Z^0 boson decays into two particles in the lowest order, the scattering angle Θ is easily defined as the angle of incoming antiparticle (e^+) and the outgoing antiparticle (μ^+). To measure the values

$$N_+ \equiv \int_0^1 \frac{\mathrm{d}\sigma}{\mathrm{d}\cos\Theta}\,\mathrm{d}\cos\Theta \tag{5.23}$$

$$N_- \equiv \int_{-1}^0 \frac{\mathrm{d}\sigma}{\mathrm{d}\cos\Theta}\,\mathrm{d}\cos\Theta, \tag{5.24}$$

we limit the values to $\cos\Theta \in [0,1]$ and $\cos\Theta \in [-1,0]$ accordingly and in the case of the detector data we also apply the muon cuts defined in Tab. 7. The remaining number of events is then the value for $N_\pm$. Furthermore we, as before, assume a Poisson-distribution for the N, meaning $\sigma_N = \sqrt{N}$. It thus follows, according to error propagation, for the error of the asymmetry value

$$A = \frac{N_+ - N_-}{N_+ + N_-} \tag{5.25}$$

$$\begin{aligned}\sigma_A &= \sqrt{\left(\frac{\partial A}{\partial N_+}\sigma_{N_+}\right)^2 + \left(\frac{\partial A}{\partial N_-}\sigma_{N_-}\right)^2} \\ &= \sqrt{\left(\frac{2N_-}{(N_+ + N_-)^2}\sigma_{N_+}\right)^2 + \left(\frac{2N_+}{(N_+ + N_-)^2}\sigma_{N_-}\right)^2}.\end{aligned} \tag{5.26}$$

	N_+	N_-	A_{FB}^{peak}	$\sin^2\Theta_W$
Data 1	1805 ± 42	1858 ± 43	$-0.01 \pm 0,02$	0.23 ± 0.01
Data 2	1213 ± 35	1198 ± 35	0.01 ± 0.02	0.24 ± 0.02
Data 3	1233 ± 35	1321 ± 36	-0.03 ± 0.02	0.223 ± 0.008
Simulation	45103 ± 212	44700 ± 211	0.004 ± 0.003	0.240 ± 0.004

Table 17: Measured values for the asymmetry in the peak A_{FB}^{peak} with calculated errors for three data sets (*Data 1-3*) and the Monte-Carlo simulation (*Simulation*) data. Note that the values are rounded according to the leading order of the error, but the calculations are made with the exact results, also in case of $A_{FB}^{peak} < 0$ we took $-A_{FB}^{peak}$ for the calculations.

With the value A_{FB}^{peak} it is then possible to acquire a value for $\sin^2\Theta_W$ according to eq. (2.10). Error propagation then yields

$$\sin^2\Theta_W = \frac{1}{4}\left(1 - \sqrt{\frac{A_{FB}^{peak}}{3}}\right) \tag{5.27}$$

$$\begin{aligned}\sigma_{\sin^2\Theta_W} &= \frac{\partial \sin^2\Theta_W}{\partial A_{FB}^{peak}} \\ &= \frac{1}{8}\frac{1}{\sqrt{3A_{FB}^{peak}}}\sigma_{A_{FB}^{peak}}\end{aligned} \tag{5.28}$$

We examined three data sets (as opposed to only one like in the previous parts) and the simulation data with these formulas and obtained the results shown in Tab. 17. We thus have a mean value for the data sets of

$$\sin^2\Theta_W = 0.23 \pm 0.01. \tag{5.29}$$

If we compare this to the value given in the booklet of the particle data group $\sin^2\Theta_W \approx 0.2312$[PDG14] and the one obtained from the simulation , we see that the experimentally found value with our own cuts is in the 1σ range of both of those values.
The negative values that occur for the data sets 1 and 3 in Tab. 17, may seem surprising at first as the eq. (5.27) implies positive values A_{FB}^{peak}, for the value of Θ_W to be real. But this is easily mended by replacing A_{FB}^{peak} with its absolute value. The difference physically is that a positive value for A_{FB}^{peak} implies mostly forward scattering, that means the angle between the incoming e^+ and the outgoing μ^+ is $\Theta \in [-\frac{\pi}{2}, \frac{\pi}{2}]$, while negative values imply

mostly $|\Theta| \in [\frac{\pi}{2}, \pi]$. Classically we expect forward scattering to be much more probable and thus A_{FB}^{peak} to always be positive, but since in this case the incoming particles are completely annihilated and no information other than the information relevant for the conservation laws are conserved, there is no reason to assume this quantum mechanically. Moreover there is no reason to assume that the antiparticle has to scatter with the corresponding antiparticle. A negative value of A_{FB}^{peak}, can be interpreted as a positive A_{FB}^{peak} value for the angle between the incoming antiparticle and the outgoing particle. It thus is sensible to replace A_{FB}^{peak} with its absolute value in the calculations. This assumption is further reinforced by the obtained values being close to the expected values of $\sin^2 \Theta_W$ and the fact that the theoretical calculations of the asymmetry in Tab. 3 yield negative values (even though it is not at the resonance peak, the argument still holds).

6 Conclusion

In this experiment we have measured the fundamental properties of the Z^0-boson, i.e. the mass m_Z, the total decay width Γ_Z and its partial widths Γ_f. For the mass we found a value of

$$m_Z = 91.26\text{GeV} \pm 0.02\text{GeV}. \tag{6.1}$$

This is in the 4σ range of the published values of the particle data group (91.1876 ± 0.0021 GeV), which is not accurate enough to confirm previously measured values of other groups.
For the total width we found a value of

$$\Gamma_Z = 1.96\text{GeV} \pm 0.03\text{GeV}. \tag{6.2}$$

Which is in the 18σ range of the value published by the particle data group (2.4952 ± 0.0023 GeV). This measurement also does not confirm this value. This urges the question for the exactness of this measurement.
We were not able to confirm the concept of lepton universality as the values for the peak cross sections differed by up to $0.854nb$ which corresponds to 25.5% of the highest measured peak cross section (σ_μ see Tab. 15), as opposed to the expected same values for each decay channel. It is notable though that the average of the three leptonic peak cross sections

$$\sigma_l^{peak} = 2.02 \pm 0.02 \text{ nb}, \tag{6.3}$$

is in the 4σ-range of the theoretical value (2.093 nb) and thus is closer to the expected value, than the breach of the lepton universality would make

one expect. This leads to the interpretation that the errors on each channel average each other out, i.e. our cuts might not have been exact enough on the individual leptonic channels but in total the errors caused by this are averaged out.
We also measured the number of neutrino generations and obtained a value of

$$N_\nu = 3.9 \pm 0.5. \tag{6.4}$$

This is in the 2σ range of the expected value of $N_\nu = 3$, but as the error is 13% of the value itself this can not be considered a good measurement value.
Finally we measured the value for the forward backward asymmetry of the muon decay channel for the Z^0-boson, used it to calculate the squared sine of the Weinberg-Angle and obtained a value of

$$\sin^2 \Theta_W = 0.23 \pm 0.01, \tag{6.5}$$

which is in the 1σ range of the value published by the particle data group (0.2312) with a relative error margin of 0.04%, we can thus consider our measured value a confirmation of the published value.
To summarize it can be said that a new measurement with more delicately defined cuts might yield results closer to the expected values. Another source of error could be the angle ranges that have been explicitly excluded in the electron measurements, because the detector has a construction error in these ranges, have been implemented in the other decay channels. While this does not seem to have a particular effect on the quality of the measured values as the measured values for the electron channel are less exact than e.g. the measured values for the tauon channel, in which we have implemented the whole angle range, the possibility still exists that excluding those faulty angle ranges might improve the values for the other event channels. Especially the values for Γ_Z and the concept of lepton universality, which are widely undebated, would require our measurement to be remade in order to correspond to the expected results. We have been able to mostly confirm otherwise the values for m_Z,σ_l^{peak} and $\sin^2 \Theta_W$.
This whole experiment is based on the assumption that the standard model of physics is the most basic model of particle physics, i.e. we have massless neutrinos (because of which these are 'invisible' channels in the detector), 3 charged lepton generations, 3 quark doublet generations and neutral current interactions that only have Z^0-bosons and photons as exchange particles. Without these assumptions (by replacing the number of charged lepton generations with N_l for example) we would not have been able to yield any results and empirically the standard model has shown great fidelity as a model for

description of particle collisions, even though it has been shown that neutrinos do carry a relatively small mass. Another fundamental assumption is that the data provided from OPAL was measured with great precision and the Monte Carlo simulation fit those measurements very well e.g. with a very small p value for the corresponding χ^2 calculation. Also and finally, as we did not write the script ourselves, which fit the Breit-Wigner curves to the measured values, we just assumed that it did the best possible fit.

References

[OPAL] CERN (n.d.), The Opal Detector. Retrieved from: `http://opal.web.cern.ch/Opal/tour/detector.html` (on February 18$^{\text{th}}$).

[PDG14] K.A. Olive et al. (Particle Data Group), Chin. Phys. C, 38, 090001 (2014) and 2015 update.

[ROOT] CERN (n.d), ROOT. Retrieved from: `https://root.cern.ch/` (on March 3$^{\text{rd}}$).